Manuscript published on pages 50 – 65
in: A.K. Singh (ed.): Advanced X-Ray Techniques in Research and Industry.
IOS Press, Amsterdam 2005, ISBN 1-58603-537-1

Texture Mapping by Scanning X-Ray Diffraction and Related Methods

R.A. Schwarzer
Institut für Physik und Physikalische Technologien der TU, Leibnizstr. 4
D-38678 Clausthal-Zellerfeld, Germany

Key words: Energy dispersive X-ray diffraction (ED XRD), local texture, lattice strain, X-ray fluorescence micro-analysis (micro XFA), X-ray pole figures.

Abstract

Scanning X-ray mapping based on energy dispersive X-ray diffraction is an ingenious new technique for materials characterization. Texture, lattice strain as well as element distribution maps can be acquired at the same time by analyzing the intensity and shape of diffraction peaks and by measuring the count rate of characteristic fluorescence lines. Heterogeneities in the microstructure can be easily recognised by attributing pseudocolors to the image points that are specific for the measured peak intensities under consideration. Several X-ray pole figures as well as texture distribution maps for different hkl reflections can be acquired simultaneously. It is not necessary to adjust the sample on a focusing circle. Due to the large depth of focus with a collimated primary beam, rough surfaces can be imaged. The size of the measured area is only limited by the travel of the stage. Bulks can be studied irrespective of their conductivity. X-ray mapping is a very gentle method, since the specimen is only exposed to X-rays and stays in the atmospheric environment. At present, spatial resolution is in the range of some 10 μm.

1. Introduction

Almost all X-ray analysis in the laboratory is *integrating* over macroscopic scales and is *non-imaging*, i.e. the acquired diffraction patterns as well as the fluorescence X-ray spectra, and hence the information on crystallography and element composition are an average over the whole illuminated wide sample area. Material properties of solids depend on the shape and arrangement of the crystallites constituting the microstructure and on the concentration of elements, but in particular on the spatial distribution of phases, on the distribution of grain orientations ("crystal texture"), on the character of grain respectively phase boundaries, on lattice defects and residual stress. Inhomogeneities in the sub-millimeter range of morphology, texture, residual stress and element composition may result in similar local variations of materials properties. They are quite common in natural and in man-made materials. Texture has to be accessed in quantitative microstructural analysis since it bears information about the history of materials processing and use, of rock-forming and sedimentation.

Material's homogeneity is often decisive to the reliability and performance of an industrial product. Therefore a microstructural analysis is required beyond spatial resolution of conventional X-ray diffraction (XRD) or X-ray fluorescence analysis (XFA). In many applications the knowledge of the spatial distribution of certain *crystal lattice directions* (i.e. pole densities rather than the full *crystal lattice orientation* of each grain), of residual stress gradients and estimates of the element distribution are already sufficient. If furthermore only a moderate resolution in the specimen surface is acceptable, electron microscopy with its specific limitations can be avoided.

Although electron diffraction, in particular backscatter Kikuchi diffraction in the SEM (known as "ACOM" = Automated Crystal Orientation Mapping and "Automated EBSD") has made significant contributions to the characterization of microstructure during recent years [1], it cannot fully replace XRD and XFA techniques. The dispersion, $\Delta\vartheta/\vartheta$, in XRD by far exceeds dispersion in electron diffraction, because spectral linewidth, $\Delta\lambda/\lambda$, is extremely small and the characteristic X-ray wavelengths, λ, are in the range of the lattice spacings, thus resulting in large Bragg angles, ϑ. A high accuracy in the determination of lattice constants and grain orientation is the consequence. Continuous background is almost negligible in XFA which enables a high peak-to-background signal and excellent sensitivity. X-ray techniques are comparatively gentle since the sample need not stay in a vacuum atmosphere nor is it exposed to a beam of energetic electrons. Hence radiation damage is of no concern. The requirements of sample preparation are moderate. Insulating, magnetic or wet materials are well suited for the investigation with X-rays.

2. The principles of energy dispersive X-ray diffraction

Energy dispersive (ED) X-ray diffraction is based on Bragg diffraction of a collimated "white" primary X-ray beam. If a grain fulfills the Bragg condition

$$E_{hkl} = n \cdot h \cdot c/(2 \cdot d_{hkl} \cdot \sin \vartheta_{hkl}) \qquad (1)$$

for a photon energy E_{hkl} of the primary beam at an angle of incidence, ϑ_1, due to an appropriate orientation of lattice planes {hkl} with spacings d_{hkl} , a partial ray of this beam is reflected at an angle ϑ_2 . $\vartheta_{hkl} = (\vartheta_1 + \vartheta_2)/2$ is known as Bragg angle (Fig. 1). If the illuminated specimen volume is composed of some grains with almost the same orientation, each crystallite may reflect its own partial beam E_{hkl} into the take-off angle, ϑ_2. If the "white" spectrum of primaries is sufficiently wide, it may contain several energies $E_{hkl}^{1,2,\cdots}$ which may fulfill the Bragg condition at the same time and at the same angles of incidence and reflection, but for different sets of lattice planes $\{hkl\}^{1,2,\cdots}$ belonging to other grains with different orientations. In this case, all the partial beams from the irradiated volume of the polycrystal simultaneously strike a solid state (Si(Li)) detector which is positioned at a fixed take-off angle, ϑ_2. The beams merge in the ED spectrum to form several peaks which are centered at $E_{hkl}^{1,2,\cdots}$ in the same way as the hkl diffraction peaks are in a conventional ϑ-2ϑ scan with monochromatic radiation. They are separated in the spectrum and identified by their specific energies.

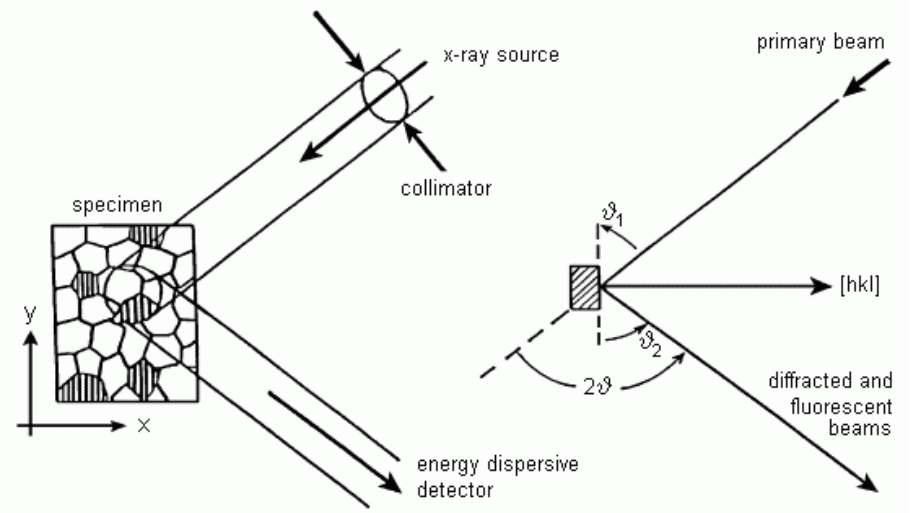

Figure 1. Schematics of the microbeam X-ray scanning instrument

In a first approximation, the intensity of an hkl diffraction peak is a measure of the volumes of all grains which have fulfilled the Bragg condition for the corresponding [hkl] lattice direction, irrespective of their arrangement and shapes in the irradiated sample volume as well as their rotation about [hkl]. However, the measured intensities are proportional not only to the volume fractions of the related grains, but also to the intensities falling in the corresponding spectral windows about $E_{hkl}^{1,2,\cdots}$ of primary X-ray radiation. They are further affected by the (spectral) absorption of the X-rays on their way from the source to the detector and by possible non-linearities of the detector system. Absorption is in particular significant within the sample. So corrections have to be applied to the measured pole intensities to relate them quantitatively to the corresponding volume fractions in quantitative texture analysis.

Pole figure measurement using a one-dimensional detector, such as a proportional counter or an ED detector, is performed by tilting the sample in small incremental steps about an axis in the diffraction plane through the angle α from 0° to about 70° and rotating the specimen about its surface normal through β from 0° to 360° relative to a coordinate system fixed to the sample. For this purpose, a special computer-controlled texture goniometer, named Euler cradle, is used. The corrected intensity values from an hkl peak are named hkl pole densities. They are stored on the hkl reference sphere of texture corresponding to the particular polar angular settings (α, β) of the specimen. An hkl pole figure is the stereographic projection of the hkl reference sphere. Since the angle of specimen tilt is limited due to excessive absorption of the beam traversing the specimen at high tilt angles, only incomplete pole figures are obtained in both modes of diffraction, in transmission as well as in backscattering. The advantage of ED X-ray diffraction is in the acquisition of *several* pole intensities $E_{hkl}^{1,2,\cdots}$ respectively hkl pole figures *at the same time* and under the same reference direction (α, β), whereas conventional pole figure measurement with monochromatic radiation and a proportional counter as the detector allows only one hkl reflection to be acquired at a time.

Lattice strain is analyzed by evaluating the shifts and widths of the diffraction peaks in the ED spectrum [2]. The angular shift, $\Delta\vartheta$, of a diffraction peak, ϑ_{hkl} , as compared to the peak position ϑ_0 from a relaxed specimen with lattice spacing d_0 , follows from Bragg's equation:

$$\Delta\vartheta = \vartheta_{hkl} - \vartheta_0 = - \tan \vartheta_0 \, (d_{hkl} - d_0)/d_0 \, , \qquad (2)$$

or transformed to the scale of photon energy, E, which is more adequate for energy dispersive diffraction:

$$\Delta E = E_{hkl} - E_0 = -E_0 \, (d_{hkl} - d_0)/d_0 \quad . \qquad (2a)$$

The energy shift is extracted on-line from the diffraction pattern after background correction by line profile analysis which is performed by fitting Gauss peaks to the measured peaks. The width of a diffraction peak reflects the variations of lattice spacing, Δd, respectively residual strain and strain gradients across grains or microstructural imperfections in the grains (residual stress of the second and third kind) in the diffracting volume. For a (semi-) quantitative estimate it is common practice to take, under the same experimental conditions, the differences of the full widths at half maximum (FWHM) of the line profiles and center line positions from the strained and from an annealed reference specimen, respectively, as a measure of residual strain. The primary beam, however, has to supply a continuous energy spectrum with constant intensity at least over a width ΔE according to Equ. 2a, since the width of the measured diffraction peak in the ED spectrum is the convolution integral of the width of the diffracted reflection ΔE due to lattice strain with the energy profile of the primary beam, the angular profile of the primary beam, the acceptance aperture of the detector and the energy resolution of the detector. The experimental

parameters have to be well adjusted by using continuous background radiation for exciting the reflections, a sufficient collimation of the primary and diffracted beams and a high energy resolution of the detector. A well collimated parallel primary beam and a narrow (Soller slit) collimator on the diffracted beam side in front of the detector can drastically improve $\Delta d/d$ resolution, but at the expense of intensity and necessary dwell time per pixel.

In the present version of the X-ray scanning instrument, the sensitivity and the $\Delta d/d$ resolution of residual strain measurement are finally limited by the spectral resolution of the solid-state spectrometer system. The standard Si(Li) detector used here has a nominal energy resolution of 140 eV at 8.4 keV (Mn Kα line). Furthermore, a tradeoff has to be made between intensity and peak width by using wide primary beam and detector apertures. They are adjusted by using appropriate pinhole diaphragms in the primary beam and an appropriate distance of the Si(Li) detector from the specimen. The apertures, $\Delta\vartheta$, of the primary and secondary beams are not crucial, unless lattice strain mapping is of concern. Since texture in most materials is hardly ever sharper than a few degree, a width of diffraction peaks in this range, according to $\Delta\vartheta$ in Equ. 2, is quite acceptable. At $2\vartheta = 40°$ (corresponding to $E_{hkl} \approx 10$ to 13 keV for low index planes of metals) apertures of 0.35° produce a FWHM between 400 eV and 500 eV which is distributed over about 100 spectral channels. Peak position is not affected by the aperture size in a symmetric goniometer setup ($\vartheta_1 = \vartheta_2$). By a Gauss fit, the peak center can so be located to $\Delta E \leq 0.5$ eV. Although the diffraction peaks in the ED spectrum are considerably broadened by the acquisition system, residual strains of the first and second kind are well resolved down to $\Delta d/d \approx 4 \cdot 10^{-4}$.

A noticeable improvement in lattice strain analysis is expected from a higher energy resolution of the detector system and a reduction of the energy interval per spectral channel. But a practical limitation still rests on the need of large apertures for gaining sufficient peak intensity. A position sensitive detector (PSD) with a standard Bragg-Brentano setup and monochromatic radiation is still superior over an ED detector by one order of magnitude or more as far as a high dispersion $\Delta d/d$ is of concern for residual strain analysis. A PSD setup enables a reliable peak-width analysis and so it will allow the mapping of residual strain distributions even of the third kind. The replacement of the ED system, however, by a PSD excludes simultaneous acquisition of several hkl peaks at the same time. Furthermore, a PSD does not enable the acquisition of X-ray fluorescence lines nor XFA nor element mapping, and imposes stringent restrictions on the flatness as well as the adjustment of the sample position since the focusing condition for the Bragg-Brentano geometry has to be matched.

X-ray fluorescence lines in the ED secondary spectrum are discriminated from diffraction peaks by their characteristic energy. If the Bragg angle is moved from ϑ_{hkl} to ϑ_{hkl}*, the centers of the diffraction peaks on the ED spectrum shift from energy channels E_{hkl} to E_{hkl}*, according to Equ. 1, whereas characteristic X-ray lines, which are scattered from the primary radiation and in particular fluorescence lines from the specimen, stay on fixed positions on the energy scale. In addition, diffraction peaks are typically much broader than characteristic lines which are not affected by the apertures of neither the primary nor the diffracted beams, nor by lattice strain. Diffraction peaks can so easily be discriminated from characteristic lines. A specific fluorescence line can be enhanced by using an X-ray tube with an anode containing an element about two positions higher in the periodic table than is the element to be detected in the sample. Likewise, a weak diffraction peak can be considerably enhanced for texture mapping as well as for pole figure measurement – but not for strain mapping – by adjusting the Bragg angle such that the energy of the diffraction peak coincides with the energy of a characteristic line in the primary beam spectrum. With these characteristics in mind, diffraction peaks, lattice strain, and X-ray fluorescence lines for element analysis can be acquired and evaluated simultaneously with an

energy dispersive system. Windows (Regions of Interest, ROI) of appropriate widths are placed on the centers of selected hkl diffraction peaks and characteristic lines in the same way as is common practice in EDS element analysis to integrate the count rates and map element distributions.

Fig. 2a shows the energy dispersive X-ray spectrum from a copper tube at 35 kV accelerating voltage, and Fig. 2b the ED diffraction spectrum from a cross rolled AlMn1 specimen using the same primary beam radiation. In both spectra the characteristic copper Kα and Kβ lines are present. Characteristic fluorescence lines from aluminum are not contained in the spectrum of Fig. 2b although aluminum is weekly excited by the primary beam, since this soft X-ray radiation of 1.5 keV is absorbed by air on the path from the sample to the detector. The small content of 1% manganese, however, is strongly excited by copper radiation to emit Mn Kα and Mn Kβ fluorescence lines of 5.9 keV resp. 6.5 keV which are seen to form two sharp peaks on the low energy side of the spectrum. At the high energy side, starting from the characteristic copper K lines, a set of relatively broad diffraction peaks can be identified. The low-index peaks are separated in the spectrum, and no peak overlap occurs for 200, 220, 400, 331 and 422 reflections, whereas the 222 and 311 peaks are coincident with each other. The individual peak intensities differ significantly from tabulated powder diffraction intensities. The differences are an indication of preferred crystal orientations in the rolled aluminum sheet. The 111 peak at a position close to Mn Kβ, for instance, is missing at all due to the specific texture.

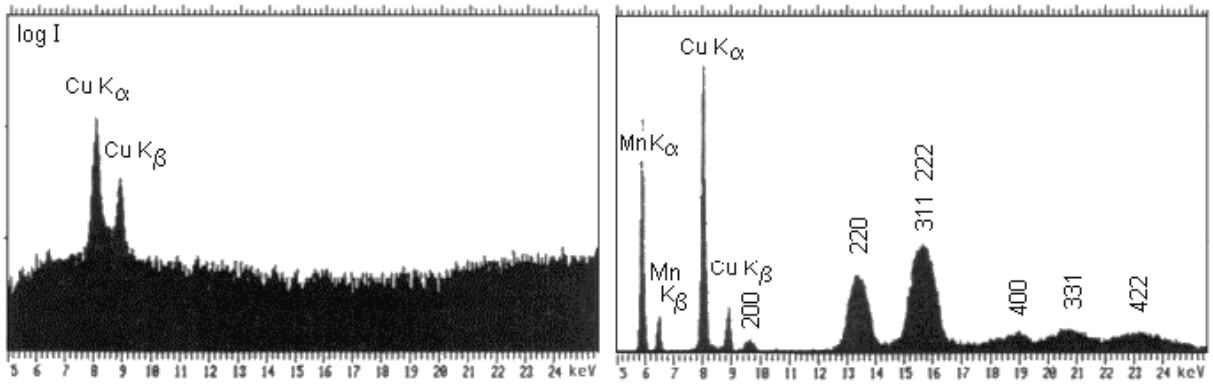

a. Primary beam spectrum(Cu, 35 kV) (logarithmic intensity scale)

b. Cross-rolled aluminum sheet (linear intensity scale)

Figure 2. Energy dispersive X-ray spectra

Spatial resolution of ED X-ray diffraction and fluorescence analysis is limited by the size of the X-ray spot on the tilted specimen surface. Synchrotron radiation is an ideal source for obtaining an extremely bright and small X-ray probe [3], but the limited availability of synchrotron facilities still demands for using conventional X-ray generators as a more feasible alternative in the laboratory. Since no conventional lenses are available for white X-rays, a beam collimator has been used for the present XSI which consists of two small circular diaphragms. The main drawback of a diaphragm collimator is the loss of intensity. An increase in spot brightness is expected from glass capillary collimators [4, 5] which would enable a higher spatial resolution or a shorter acquisition time. Capillary optics, however, have a filtering effect on the primary beam energy which might be adverse to ED diffraction.

The oblique incidence of the primary beam results in an elliptical foreshortening of the spot on the sample surface. Spatial resolution decreases with angular tilt, γ, of the specimen with respect to the incoming beam. A circular primary X-ray spot is elongated by projection on the tilted

specimen surface to an ellipse of aspect ratio 1/cosγ, whereas at shallow incidence the depth of penetration beneath the surface is reduced and surface sensitivity is improved. A practical limit of spatial resolution is presently at 0.1 mm for pole-figure measurement and lattice strain mapping, and 0.05 mm for element and texture mapping, due to the low intensity of the collimated primary beam.

Absorption in air must be considered for quantum energies $E_X < 3$ keV. Hence, a Helium atmosphere or an evacuated specimen chamber will be indispensable if materials with large lattice constants have to be studied by ED XRD as well as light elements have to be detected by XFA. Very high quantum energies, on the other hand, are not adequate, since with hard X-rays Bragg´s angles decrease unduly up to grazing incidence. Then the spot size is extremely foreshortened and spatial resolution is impaired. A high excitation of fluorescence lines is obtained with an overvoltage of the primary beam of about twice the energy of the characteristic lines of the elements to be detected. A good compromise for most samples in reflection mode is obtained with an angle of incidence of $\vartheta_1 \sim 45°$ and quantum energies of the primary beam between 8 keV and 15 keV.

3. The X-ray scanning instrument based on a conventional X-ray source and ED spectrometry

The X-ray *S*canning Instrument (XSI) [6 - 8] combines three techniques based on ED diffraction that are spatially resolved pole figure measurement as well as, on a grain-specific level, texture mapping and lattice strain mapping. The fourth technique is element mapping by X-ray micro-fluorescence analysis. Although applications have initially been focused on metals and their response to plastic deformation, a wide field regarding deformation of rocks and minerals in general can be tackled as well.

To obtain images of the morphology, the spatial distributions of elements, the type of crystal lattice (i.e. phases), grain orientations and residual lattice strain from the same localized specimen area requires a mapping technique whereby an X-ray beam of small spot size is generated, and the specimen is mechanically scanned under the stationary beam spot. In our design, shown in Fig. 3, the XSI consists of a conventional X-ray source (PHILIPS generator PW 1830/25) equipped with a fine-focus tube. Most applications have been carried out with a tungsten anode in order to obtain a high intensity of continuous radiation. The "white" primary radiation is not filtered. Therefore almost no practical restrictions have been imposed on lattice spacings for diffraction, and a wide range of elements can be excited to fluorescence emission. A circular pinhole collimator is used to produce a small primary beam spot. On the two-circle goniometer base (PHILIPS PW 1835), an open Euler cradle (PHILIPS X'Pert MRD goniometer) with a stepping-motor driven x-y-z sample stage is mounted which allows the sample to be translated in 1 μm wide steps over an area of 100 mm by 100 mm. The diffracted secondary spectrum is acquired with an energy dispersive solid state spectrometer system (SPECTRACE 6100 and TRACOR NORAN Si(Li) detector) which contains diffraction and X-ray fluorescence peaks for mapping. As an alternative, particularly for pole figure measurement and lattice strain mapping, a conventional proportional counter respectively a position sensitive detector can be used, with a Kβ filter either in the primary beam or in the diffracted beam right in front of the detector. The proportional counter and the position sensitive detector have to be set to the appropriate ϑ–2ϑ positions for each measured hkl pole figure separately.

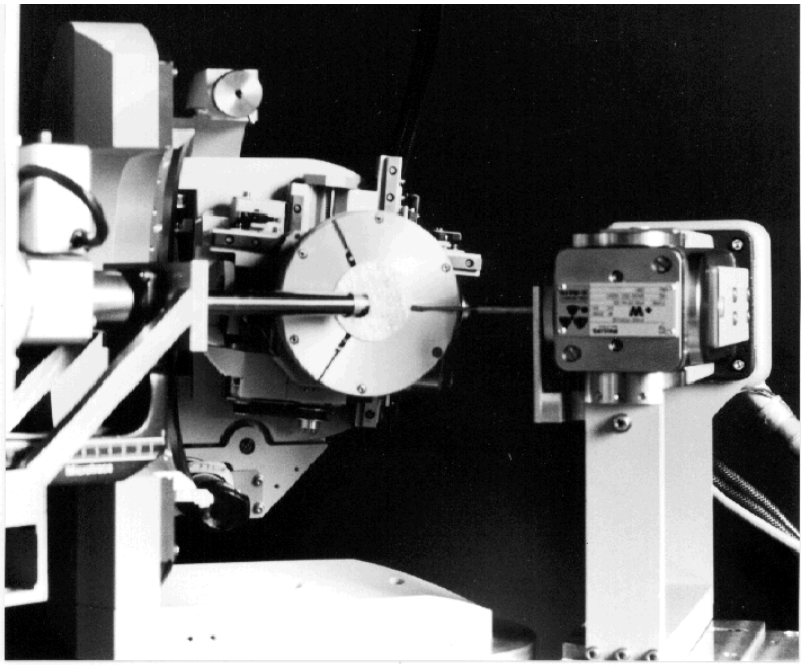

Figure 3. The experimental setup of the X-ray scanning instrument.

The instrument is under the full control of a personal computer. The specimen is translated step by step with the x-y stage across a user defined grid pattern, e.g. on scans along a line or on regular raster grids of rectangular or polygon shape up to 100 mm by 100 mm wide, in order to match the scanned field to the area of interest. Usually constant step widths in x and y direction are chosen. The current sample position under the beam spot is monitored with a video camera, and so the corner points of the sampled region are defined conveniently.

Pole-figure measurement has to precede texture mapping on the same specimen area in order to find out the significant texture components. Thinned angular grids, equal area grids or relevant sections on the pole sphere can be selected to reduce acquisition time. Pole-figure measurement can be combined with a controlled spatial x-y translation of the specimen and integration of the pole intensity for this specimen area.

Large specimen tilts require the correction of peak intensities for background. They may also result in inconsistent pole-figure data if texture is not uniform in depth beneath the shallow surface, since X-ray diffraction becomes more surface sensitive with decreasing angle of incidence. Any specimen reference direction (α, β) can be chosen for mapping provided that pole density (i.e. diffracted intensity) is high enough – which of course depends on local texture. It is worth noting that texture as well as residual strain are probed exclusively for those grains only which satisfy the Bragg condition for the selected specimen-fixed reference direction. There is no intensity at all acquired from grains with other orientations.

A comprehensive PC software package has been developed [2, 8]. One part contains the hardware control of the goniometer, the Eulerian cradle, the x-y-z sample stage and the proportional counter as well as the EDS system. The other part has been developed for the graphical representation of measured pole figures and for mapping the microstructure by attributing pseudo-colors to the pole densities (“texture mapping”), the shift and width of the diffraction peaks (“lattice strain mapping”) respectively the intensities of selected fluorescence lines (“element mapping”).

Modern X-ray texture goniometers are often equipped with a computer-controlled x-y specimen stage on the Eulerian cradle. They enable, in principle, texture mapping, if appropriate software is available for controlling the mechanical x-y sample scan, the acquisition, interpretation and representation of the diffraction data. Spatially resolved texture analysis has been demonstrated on a commercial X-ray texture goniometer by calculating off-line orientation densities, texture symmetry, texture index and the Taylor factor in several raster points [9]. X-ray microbeam scanning instruments for imaging XFA have demonstrated their high potential since many years [10 - 13], and commercial systems have been developed [14, 15]. The combination of these techniques in one instrument, however, is a unique feature of the XSI.

4. Examples of application

a. Texture mapping

Compression induces a change of texture in the material which depends on the degree and rate of plastic deformation. By impressing the jaws of a mechanical testing machine into the coarse grain surface of a recrystallized aluminum sheet metal, a rhombic relief pattern has been formed. The sample was then mechanically ground and polished to a flat mirror such that the pattern was no longer visible. The compression process, however, has changed local texture. In the texture maps (Fig. 4) high pole densities can be seen in regions where the corrugating teeth of the jaws caused a high local deformation, whereas deformation in the grooves of the jaws was low enough to preserve the original texture of the metal sheet [7]. The texture maps of Fig. 4 were acquired at symmetrical diffraction settings ($\vartheta_1 = \vartheta_2$) simultaneously from the same sample area. Hence the spatial distributions of pole densities of the lattice planes (200), (220), (311) and (222), respectively (331) *in sheet normal direction* are shown. The sheet texture did not contribute to these selected diffraction peaks. If a certain texture component of the metal sheet is of interest, the specimen has to be tilted away from the symmetrical geometry to an appropriate pole-figure point into which the sheet is diffracting. The corresponding angles of tilt can be read from X-ray pole figures that have to be acquired in advance.

An important industrial application of zinc is hot galvanizing of steel sheet metal. In the zinc bath a layer of Fe-Zn alloy is formed on the surface of the workpiece which is covered by liquid zinc. When this coating solidifies, a characteristic pattern known as "zinc flower" is visible which is composed of zinc grains of varying orientations. The crystal texture of the zinc coating has an effect on mechanical properties as well as corrosion resistance of the galvanized material. Hence local texture is of some practical importance. In texture maps of the surface the spatial variation of pole densities can be recognized (Fig. 5) [7]. The zinc flower contains clusters of grains which are stretched out in the rolling direction of the sheet substrate. Grain clusters with (10-10), (10-11) and (0002) planes parallel with the specimen surface are clearly visible in the texture maps.

Fig. 6 shows the ED X-ray spectrum from an image point of Fig. 5. It is composed of characteristic K lines from copper (i.e. scattered primary radiation) and from zinc (fluorescenced by the hard fraction of continuous primary radiation) as well as diffraction peaks from zinc. The characteristic lines form narrow peaks, whilst the diffraction peaks are rather broad again, due to the wide beam aperture (see Equ. 2a) and can thus easily be discriminated. Two windows are marked by hatching which were used for the collection of the (10-10) and (10-11) texture maps. The (10-10) reflection is superimposed on the Fe Kα peak. This characteristic fluorescence line from iron, however, is only induced very weakly beneath the zinc coating, a fact which is corroborated by the absence of the Fe Kβ peak in the spectrum. Hence the FeK fluorescence background does not interfere with texture measurement in this example.

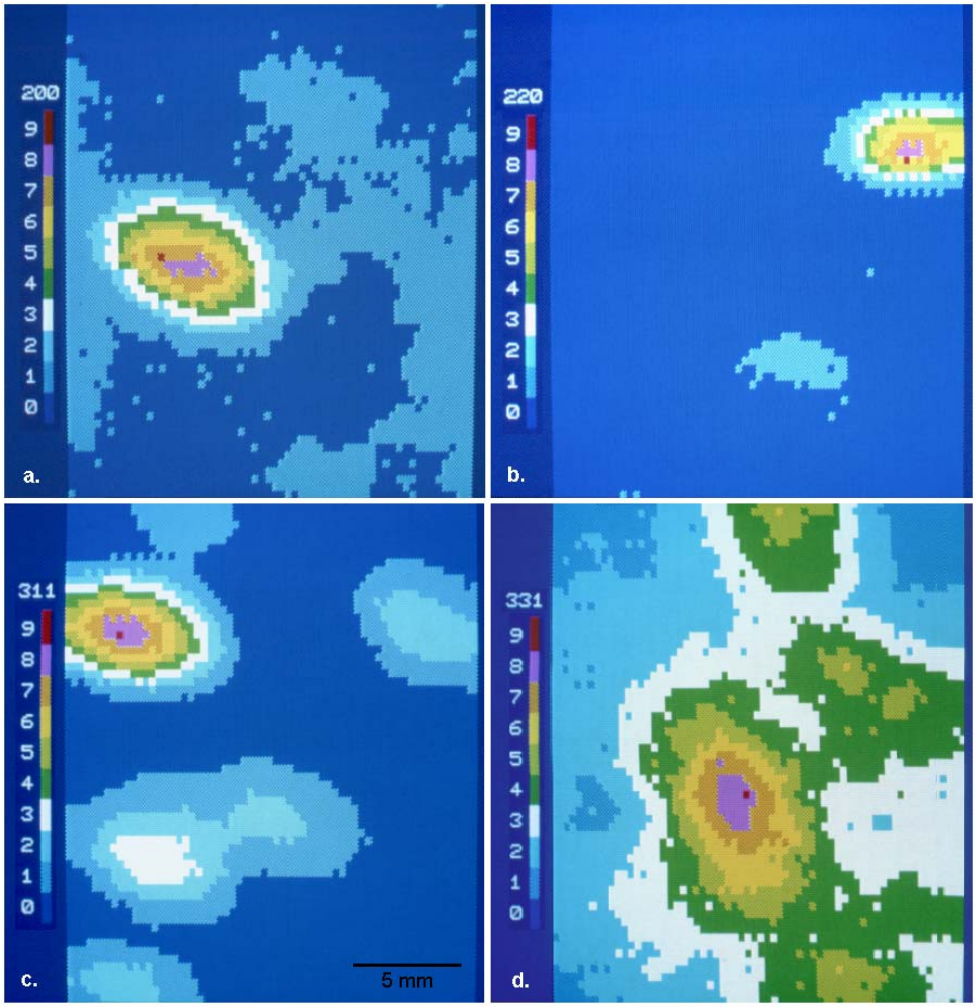

Figure 4. Texture maps of a compression pattern in aluminum revealing local plastic deformation. (a) {200} reflections b) {220} reflections c) {311} and {222} reflections d) {331} reflections

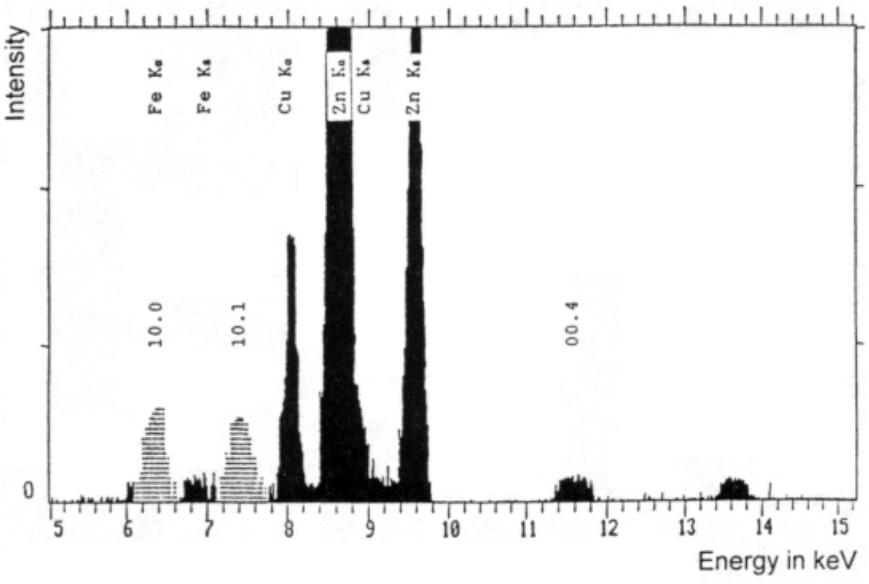

Figure 6. Energy dispersive X-ray spectrum of the zinc coating of Fig. 5.

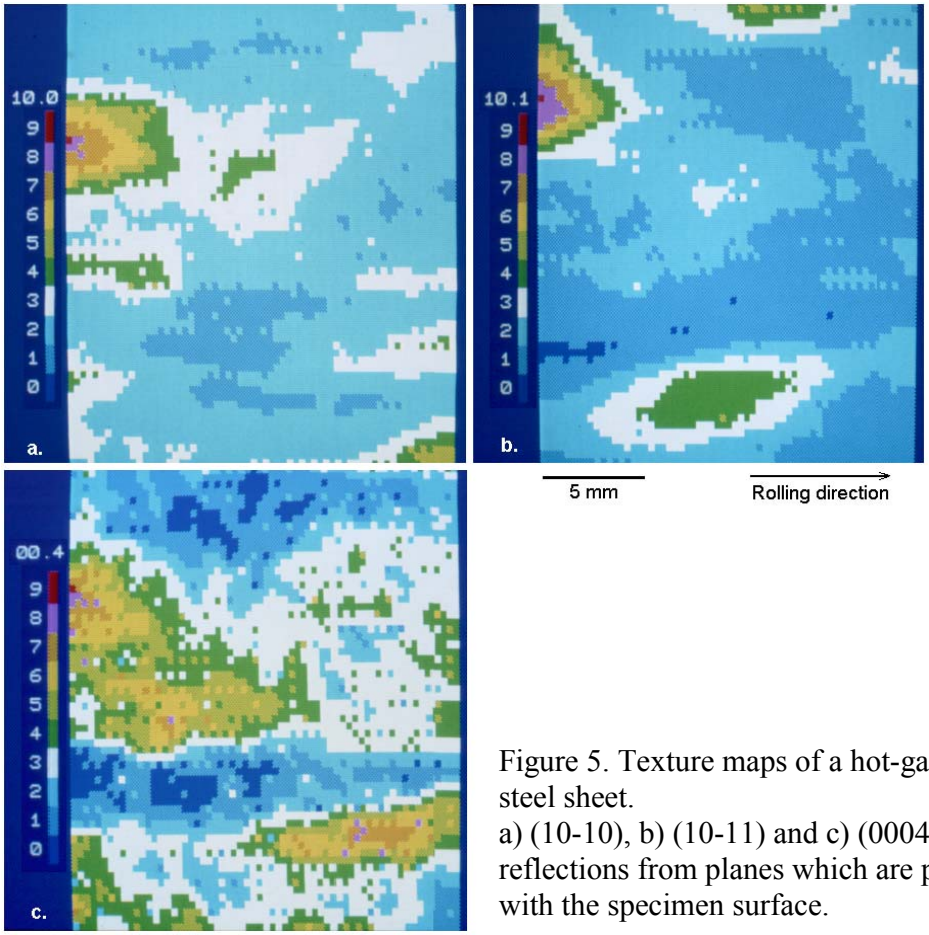

Figure 5. Texture maps of a hot-galvanized steel sheet.
a) (10-10), b) (10-11) and c) (0004) reflections from planes which are parallel with the specimen surface.

The process of metal forming is mainly dependent on the macroscopic parameters to which the workpiece is subjected such as distribution of strain, the rate and speed of plastic deformation, temperature, friction between the workpiece and the forming tool, but also on the microstructure, texture and (anisotropic) properties of the material. Finite element methods are now capable to model rather complicated forming processes, and spike forming (Fig. 7a) is a critical benchmark test in numerical modeling [16].

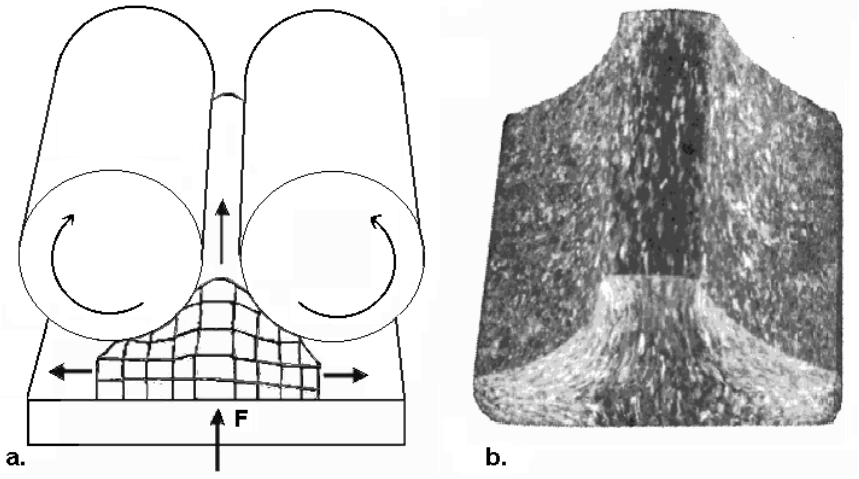

a. Schematics of the experimental setup. b. Aluminum sample after friction test.
Figure 7. The friction test by back-rolling.

Iniatially, the test specimen had a strong and uniform cube texture across the aluminum bar. After friction test rolling (Fig. 7b), pronounced texture inhomogeneities in the cross section plane are observed [17]. The cube texture is still maintained in the center plane which is parallel with the rolls (Fig. 8a). Due to the friction with the rolls and the force F, the material is subjected to heavy plastic deformation on both sides of the center plane. The grains are elongated and rotated to gradually accommodate the shape of the rolls. Crystal texture follows this change in microstructure from the center to the surface of contact with the rolls (Fig. 8b, c), and a clear inhomogeneity of local texture develops (Fig. 9a and 9b). The texture maps have been acquired in the symmetric goniometer setup ($\vartheta_1 = \vartheta_2$) (central pole-figure point P in Fig. 8a). The local distributions of grains with (200) (Fig. 9a) respectively (111) (Fig. 9b) lattice planes parallel with the cross section plane are displayed.

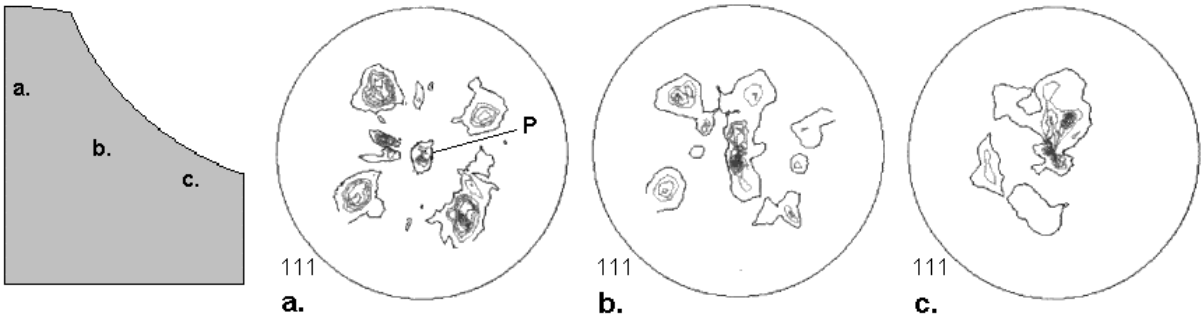

Figure 8. The texture of an aluminum sample after friction test. Experimental 111 pole figures: a. at the mid plane of the cross section, b. at quarter depth and c. close to the roll.

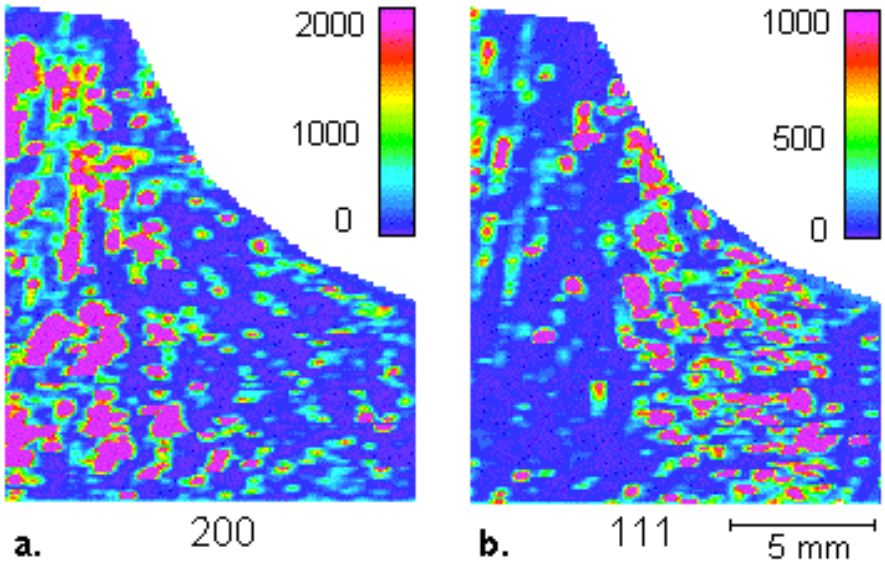

Figure 9. Texture maps of the aluminum sample after friction test show heterogeneous texture. a. Texture map for (hkl) = (200) b. Texture map for (hkl) = (111).

b. Pole figure measurement and lattice strain mapping

The cross section along the mid plane of an aluminum rivet was carefully ground and polished to a flat. A final electrochemical polishing was applied in order to remove any mechanical damage introduced during mechanical preparation. Before mapping, several pole figures have been acquired in steps along lines across the head and the bolt of the rivet to recognize relevant texture

components. A fiber texture has been found in the bolt region (Fig. 10) [2]. The experimental pole-figure data can be used for ODF analysis and for the calculation of average tensorial material properties.

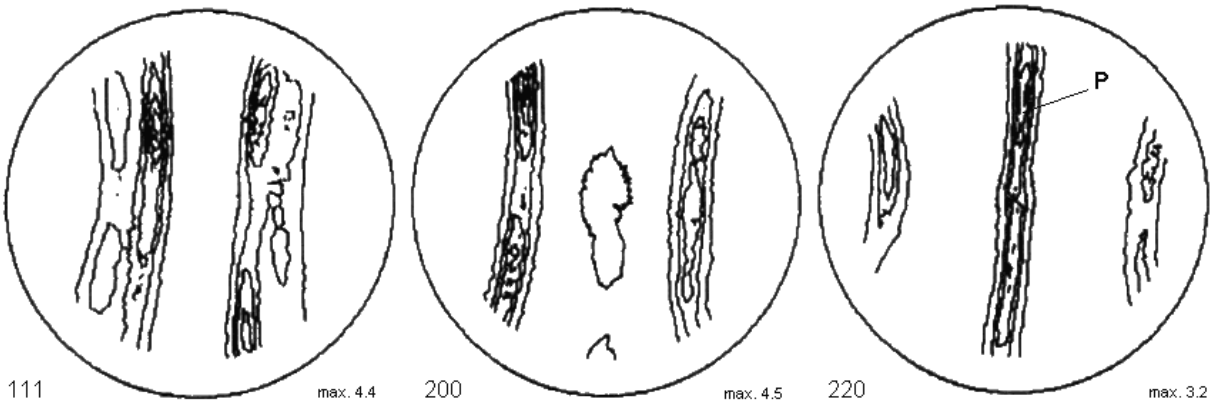

Figure 10. Pole figures acquired across the rivet bolt. The polar specimen direction P ($\alpha = 35°$, $\beta = 83°$) has been used for texture and residual strain mapping (cf. Fig. 11).

The (220) diffraction peak P ($\vartheta_1 = \vartheta_2 = 20.1°$, $E_{220} = 12.62$ keV; $\alpha = 35°$ and $\beta = 83°$) has been used for evaluating both, the spatial distributions of pole density (texture map) and residual lattice strain (residual strain map), at the same time. Because of the low diffracted intensity, dwell time had to be extended to 10 sec/pixel to obtain a sufficient count statistics. 2,232 image points at a step width of 120 µm have been acquired. A clear heterogeneity is revealed in the texture (Fig. 11a) as well as in the strain maps (Fig. 11b). Two almost parallel stripes of high pole density run along the axis of the bolt with a slight shift to the right hand side. They form a tube of about 1/3 of the bolt diameter. The head of the rivet shows a much lower density of this pole. It is worth noting that a butterfly-shaped minimum is observed which might result from punching the head during production.

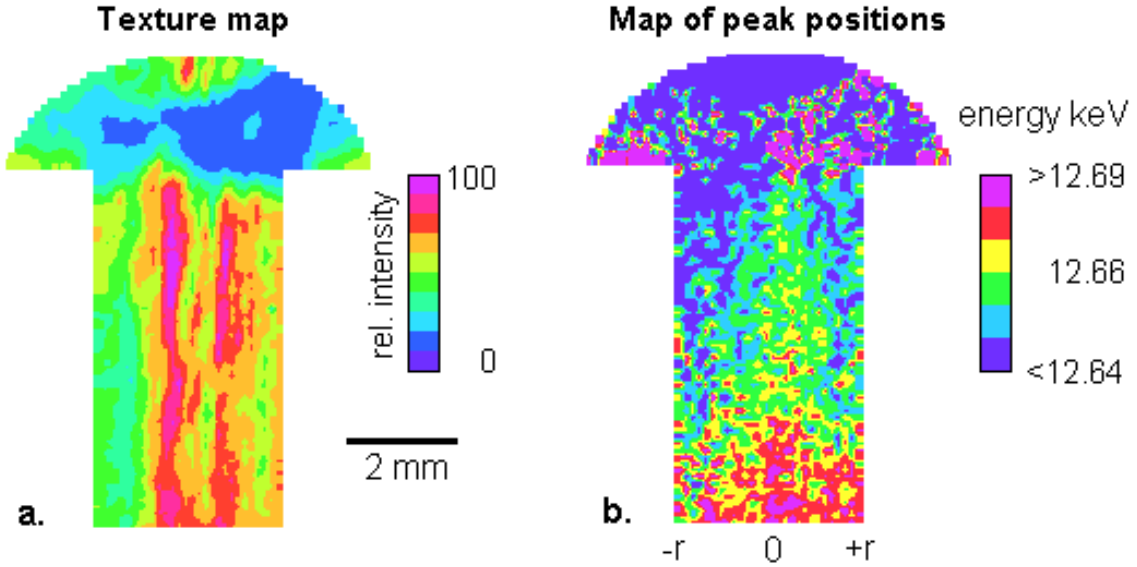

Figure 11. Cross section of an aluminum rivet. Distribution maps (a) of the intensity (pole density, texture) and (b) of the shift (residual strain) of the 220 peak at pole P ($\alpha = 35°$, $\beta = 83°$).

Along the bolt to the head there is a gradient in compressive residual strain. A dish-shaped maximum of compressive strain (dark) is found in the head which is related to the butterfly-shaped minimum in the 220 texture map. There is an increased compressive residual strain in the interior of the "texture tube" (dark) and a tensile strain (bright) to the bolt surface.

c. Imaging micro-XFA

A test specimen for imaging micro X-ray fluorescence analysis and for checking spatial resolution has been made by sputter-depositing gold through a TEM support grid on a glass substrate to form regular patches 420 µm by 420 µm wide. The annular primary beam apertures had a diameter of 30 µm. Using the Au Lα fluorescence lines for imaging, the free bars (< 60 µm wide gaps) between the patches are clearly resolved in two perpendicular directions in the XFA map (Fig. 12) [18]. A spatial resolution of <50 µm is thus demonstrated.

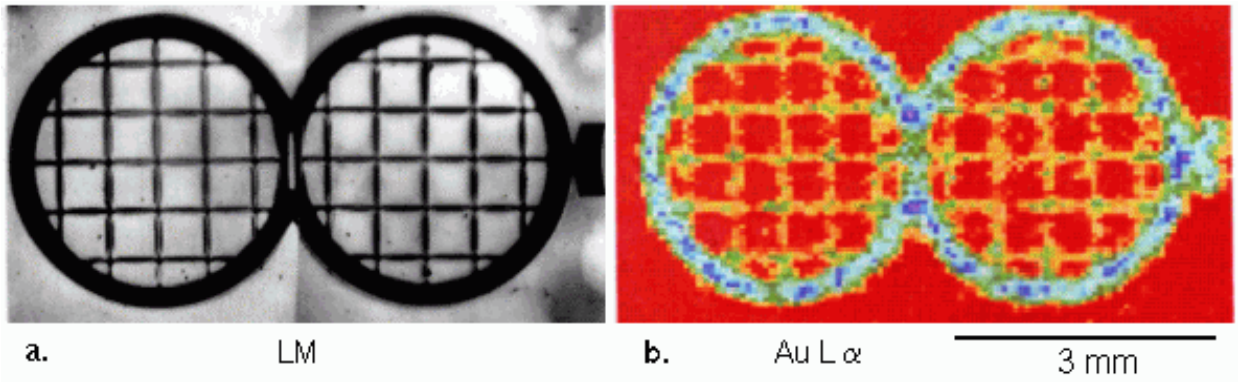

Figure 12. Gold pattern from sputtering through a TEM support grid.
a. Image in the light microscope b. X-ray micro-fluorescence map with the Au Lα line.

6. Conclusion

Scanning X-ray mapping based on energy dispersive spectrometry is a powerful technique for a comprehensive materials characterization. It combines, on a grain specific scale, simultaneous texture mapping, residual strain mapping and imaging X-ray micro-fluorescence analysis by translating the sample step by step on a user defined grid under the stationary beam spot. Pole figures are measured from selected small areas. All reflections are measured simultaneously at the same angular setting. For ED diffraction it is not necessary to adjust the sample on a focusing circle. Measurement is not affect by the degree of plastic deformation. Due to the large depth of focus with a collimated primary beam, the sample surface need not be prepared to a plane and sample preparation is not difficult. Often a thorough cleaning of the surface is adequate. X-ray mapping is a very gentle method, since the specimen is only exposed to X-rays and stays in the atmospheric environment. Bulks can be studied irrespective of their conductivity.

Residual lattice strain as low as $\Delta a/a = 4 \cdot 10^{-4}$ is analyzed by evaluating the shifts and profiles of diffraction peaks in the spectrum using a standard ED detector. Spatial resolution of pole-figure measurement and residual lattice strain mapping is presently limited to 0.1 mm, whilst resolution of micro X-ray fluorescence element maps and of texture maps is limited to about 0.05 mm, as a consequence of the low intensity of a collimated primary beam.

References

1 R.A. Schwarzer: Automated crystal lattice orientation mapping using a computer-controlled SEM. Micron **28 (**1997) 249-265

2 A.H. Fischer and R.A. Schwarzer: Mapping of local residual strain with an X-ray scanning apparatus. Materials Science Forum **273-275 (**1998) 673-677

3 P.-C. Wang, G.S. Cargill III, I.C. Noyan, E.G. Liniger, C.-K. Hu and K.Y. Lee.: Thermal and electromigration strain distributions in 10 µm-wide aluminum conductor lines measured by X-ray diffraction. Mat. Res. Soc. Symp. Proc. **473 (**1997**)** 273-278

4 E.N. Maslen: An X-ray collimator for single-crystal goniometers. Sci. Instruments **35** (1958) 110-111

5 S. Larsson and P. Engström: X-ray microbeam spectroscopy with the use of capillary optics. Advances in X-ray Analysis **35 (**1992) 1019-1025

6 R.A. Schwarzer: Scanning X-ray microscopy for texture mapping by energy dispersive diffraction. Proc. 12 Intern. Congr. on X-ray Optics and Microanalysis (12 ICXOM), Cracow 1989, vol. 1, pp. 205-208

7 R.A. Schwarzer: Texture distributions imaged by energy dispersive X-ray diffraction. Steel Research **64 (**1993) 570-574

8 A.H. Fischer and R.A. Schwarzer: X-ray pole figure measurement and texture mapping of selected areas using an X-ray scanning apparatus. Materials Science Forum **273-275** (1998) 255-262

9 H. Klein and H.J. Bunge: Location resolved texture analysis. Z. Metallkunde **90 (**1999) 103-110

10 P. Horowith and J.A. Howell: A scanning X-ray microscope using synchrotron radiation. Science **178 (**1972) 608-611

11 K.W. Jones and B.M. Gordon: Trace element determinations with synchrotron-induced X-ray emission. Anal. Chem. **61 (**1989) 341A-356A

12 A. Rindby, P. Engström, S. Larsson and B. Stocklass: Microbeam technique for energy-dispersive X-ray fluorescence. X-ray Spectrometry **18 (**1989) 109-112

13 D.A. Carpenter: Improved laboratory X-ray source for microfluorescence analysis. X-ray Spectrometry **18 (**1989) 253-257

14 D. Werry and B. Cross: Applications of small-area X-ray fluorescence analysis using a microbeam X-ray source. Spectroscopy International **1 (**1989) 58-59

15 D. Rammlmair, K.D. Tacke and H. Jung: Application of new XRF-scanning techniques to monitor crust formation in column experiments. In: Securing the Future, Proceedings of the International Conference on Mining and the Environment, Skellefteå 2001, Volume 2, pp. 683-692

16 M. Schönauer, T. Rodić and D.R.J. Owen: Numerical modelling of thermomechanical processes related to bulk forming operations. J. Physique IV **3** (1993) (colloque 7) 1199-1209

17 A. Fischer: Ortsaufgelöste Polfigurmessung, Texturtopographie und Mikro-Röntgenfluores-zenzanalyse. PhD Thesis, TU Clausthal (Germany) 1998

18 R.A. Schwarzer and M. Wehrhahn: X-ray scanning apparatus for mapping texture and element distributions. Textures and Microstructures **29 (**1997) 65-76